JOURNAL GEOLOGICAL SOCIETY OF INDIA
Vol.89, June 2017, pp.619-630

Modeling of Source Parameters and Moment Tensors of Local Earthquakes Occurring in the Eastern Indian Shield

Koushik Biswas and Prantik Mandal*
CSIR- National Geophysical Research Institute, Uppal Road, Hyderabad – 500 007, India
E-mail: prantik@ngri.res.in

ABSTRACT

Earthquake source parameters and crustal Q are being estimated simultaneously through the inversion of S-wave displacement spectra from three-component recordings of ten local cratonic intraplate earthquakes from 3-6 broadband stations in the eastern Indian shield, wherein, an iterative Levenberg-Marquardt inversion technique is used. The estimated seismic moment (M_o) and source radii (r) vary from 7.4 x 10^{12} to 7.1 x 10^{14} N-m and 144.2 to 211.3 m, respectively, while estimated stress drops ($\Delta\sigma$) and multiplicative factor (E_{mo}) values range from 0.11 to 4.13 MPa and 1.33 to 2.16, respectively. The corner frequencies range from 6.23 to 8.62 Hz while moment magnitudes vary from 2.44 to 3.57. The radiated seismic energy and apparent stresses range from 8.3 x 10^6 to 2.0 x 10^{10} Joules and 0.06 to 0.94 MPa, respectively, wherein the estimated corner frequencies and seismic moment satisfy the relation $Mo \infty f_c^{-(3+\varepsilon)}$ for $\varepsilon = 12.7$. Thus, the source scaling of these events clearly deviates from the self-similarity i.e. f^{-3}. Estimated Zuniga parameters reveal that all selected events satisfy the partial stress drop model, which is in good agreement with the global observations. Our estimated crustal S-wave quality factors vary from 1091 to 4926 with an average of 3006, suggesting a less heterogeneous crustal structure underlying the study region. We also perform moment tensor inversion of five selected local events using ISOLA software, which reveals that the dominant deformation mode for the eastern Indian shield is left-lateral strike slip motion with minor normal dip-slip component on an almost vertical plane. This observation suggests that neotectonic vertical movements might have played a key role in generating these earthquakes. Our modeling also depicts that the seismically mildly active Singhbhum shear zone and Eastern Ghats mobile belt are characterized by the left-lateral strike motion while two events in the Chotanagpur half graben belt suggest a normal dip-slip motion along a south dipping plane. A north-south orientation of P-axis is found to be dominant in the area, which is consistent with the prevailing north–south compression over the Indian plate.

INTRODUCTION

In general, cratons are assumed to be tectonically stable parts of the earth, which are currently not experiencing large scale seismicity. However, occurrences of intraplate earthquakes in the globe suggest that cratons do experience intraplate stresses that cause small to moderate size earthquakes (Al-Heety 2007; Calais et al. 2010; Malservisi et al. 2013). The occurrences of small earthquakes in the largest and oldest North American craton in Canada have been explained in terms of post-glacial rebound and failed rifts. Two kinds of models involving weak zones and stress concentrations can explain intraplate seismicity satisfactorily. Most of the world's significant intraplate earthquakes are found to be associated with crustal weak-zones like ancient rifts or failed rifts (Sykes 1978; Johnston and Kanter 1996) or suture zones (i.e. around craton edges as shown by Mooney et al. 2012). Occurrences of some intraplate earthquakes are also found to be associated with contrasts of elastic properties (Campbell 1978) and fault intersections (Talwani 1999; Gangopadhyay and Talwani 2003). Further, Assumpco et al. (2004) proposed that thin lithospheric spots between ancient cratonic areas can also be regarded as a weak zone but the seismicity is due to stress concentration in the elastic upper crust. Concentrations of stresses and deformation associated with craton edges can also cause seismicity e.g. Phanerozoic suture zones in North America (Lenardic et al. 2000; Mooney et al. 2012).

Most of the Indian seismicity is confined to the Himalayan frontal arc. However, earthquakes do occur in the Peninsular India. Many Peninsular Indian earthquakes have occurred in recent times e.g. 1967 M_w6.3 Koyna (M_w6.3), 1993 M_w6.2 Latur, 1997 M_w5.8 Jabalpur and 1970 M_w5.4 Bharuch and 2001 M_w7.7 Bhuj. These events have occurred in an intraplate setting, and have generally been attributed to the reactivation of pre-existing faults / weak zones in response to the prevailing N-S compression of the Indian plate or local tectonic forces like topography, crustal density heterogeneities, crustal intrusive, fluids, etc. (Gangopadhayay and Talwani 2003; Mandal et al. 1997; Krishna Brahmam and Negi 1973; Rajendran et al. 1996). However, no significant earthquakes of M≥5 have occurred in the Singhbhum craton and Chotanagpur plateau in recent times, thus, the seismicity in these regions is low. But, smaller earthquakes of M≤4.0 have been occurring in these regions regularly. Until today, no efforts have been made to study the seismogenesis of these smaller cratonic earthquakes due to lack of digital data. In 2013, the National Geophysical Research Institute (CSIR-NGRI), Hyderabad, has deployed a seismic network of fifteen three-component broadband seismographs in an area of about 300 x 500 km^2 covering Singhbhum craton, Chotanagpur plateau, and their surrounding regions, to understand the seismogenesis of cratonic intraplate earthquakes occurring in the eastern Indian shield. This network has enabled us to study the seismogenesis of smaller cratonic earthquakes occurring in these regions, through the estimation of source parameters and moment tensors of local earthquakes, which have occurred during 2013-14. In this paper, we present the estimated source parameters of ten local events and moment tensor solutions of five selected local events from the eastern Indian shield (Fig.1).

GEOLOGY, TECTONICS AND SEISMICITY OF THE EASTERN INDIAN SHIELD

Our study region is bounded in the west by the Permian, Paleoproterozoic and Gondwana basin formations and in the south by the Eastern Ghats mobile belt, Mahanadi fault, Ranipather shear zone and the recent coastal alluvium. It is surrounded in the north and east by the vast Gangetic alluvium and the Quaternary sediments of the Bengal basin (Fig.1). Our study region can be divided into three tectonic zones viz. Singhbhum craton in the south, Singhbhum orogenic belt in the center and Chotanagpur plateau in the north (Sarkar 1982). A 3.5 Ga supracrustal succession intruded by the multi-phase,

0016-7622/2017-89-6-619/$ 1.00

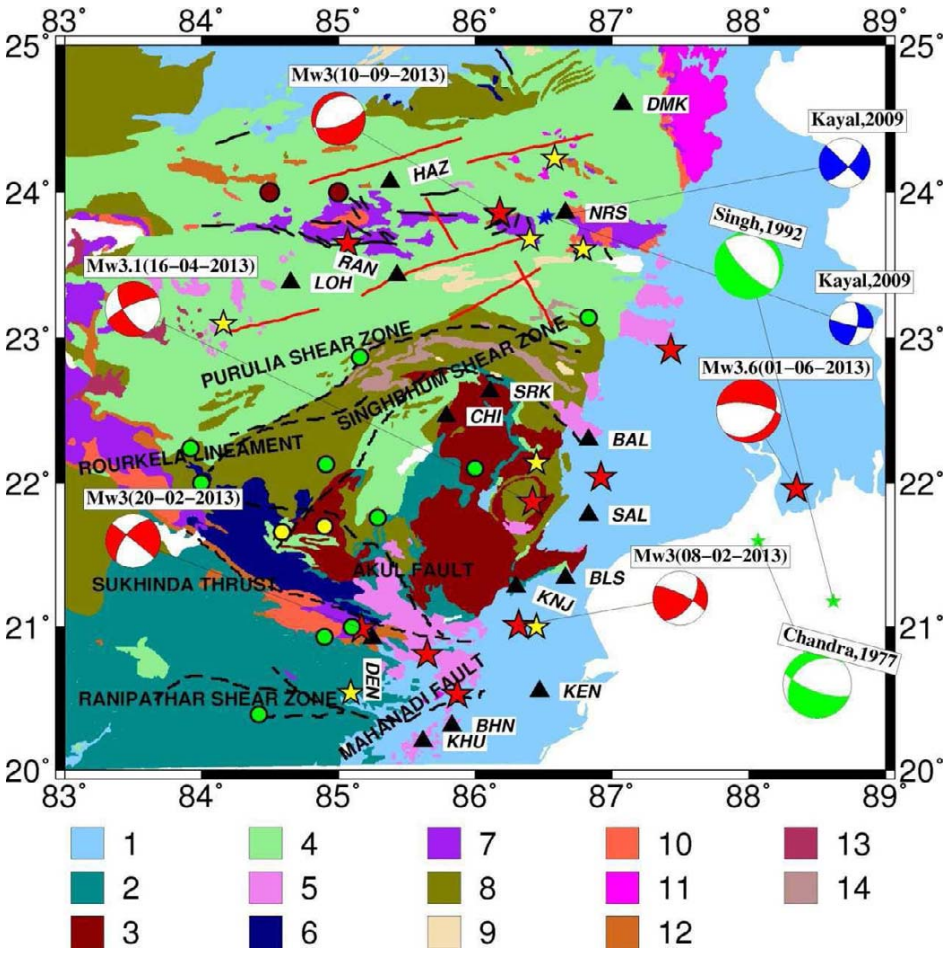

Fig.1. (1) Quaternary. **(2)** Archaean. **(3)** Singhbhum Granite. **(4)** Proterozoic. **(5)** Cenozoic. **(6)** Neo-Proterozoic. **(7)** Permian. **(8)** Paleoproterozoic. **(9)** Mesoproterozoic. **(10)** Triassic-Jurassic. **(11)** Jurassic-Cretaceous. **(12)** Talchir Formation. **(13)** Deccan Traps. **(14)** Dalma volcano. Red triangle describes the stations (KHU-Khurda, BHN-Bhubaneswar, KEN-Kendrapara, DEN-Denkanal, KNJ-Keonjhor, BLS-Balasore, SAL-Salbani, BAL-Balukuria, CHI-Chaibasa, SRK-Saraikela, LOH-Lohardaga, RAN-Ranchi, HAZ-Hazaribagh, NRS-Nirsa, and DMK-Dumka). The dotted black line represents faults; shear zone and lineament, which are written in the map. The red lines represent lineaments and black lines represent faults in the Chotanagpur plateau (upper part of the map). The yellow star represents the earthquakes which are located using single station method whereas the red stars represent the earthquakes which have been located using multiple stations. Solid brown circles mark two historical earthquakes (viz. 1968 M4.3 Hazaribagh and 1968 M5.7 Manbhum) while yellow solid circles mark two M5 events in 1863 and 1997, respectively. And solid green circles mark events of M3.0-4.9.

3.3-3.1 Ga Singhbum Granite mainly characterizes the core zone of the Singhbum craton (Mukhopadhyay et al. 2008; Acharyya et al. 2010a,b Tait et al. 2011; Mazumder et al. 2012 and references therein). Geologically, mineralogically rich Singhbhum craton comprises of granites, gneisses, quartzites, shales and phyllites, which have undergone several phases of tectonic deformation, metamorphism, and metasomatism (Dunn 1929; Sarkar and Chakraborty 1982; Acharya 1984; Ghosh and Sengupta 1990; Chetty and Murthy 1994; Saha 1994). The basement of the Singhbhum craton consists of rocks of older Metamorphic Group, comprising of predominantly schists. Relatively younger Singhbhum Group rocks and Dalma volcanics (~2.3 Ga) lie above the older Iron Ore Group rocks overlying the basement rocks. However, much younger rocks (1.0-1.6 Ga) are found in the Chotanagpur granitic gneissic terrain (CGGT), which lies north of the Singhbhum craton (Naqvi and Rogers, 1987). In addition to the Purulia shear zone, several small fractures and faults are noticed within the Damodar graben, where occurrences of small to moderate size earthquakes are also reported (Kayal et al., 2009; Mandal et al., 2017).

Small to moderate size earthquakes have been occurring in some parts of the eastern Indian Precambrian shield (Gupta et al. 2014). Two historical damaging earthquakes (viz.31 July 1868 M4.3 Hazaribagh and 30 September 1868 M5.7 Manbhum (Oldham 1883) have occurred in the Chotanagpur plateau (Kayal et al. 2009). According to USGS catalog, a significant historical earthquake of M5.2 also took place on 8 May 1963, in the Singhbhum shear zone (Fig.1). In 1964, three moderate sizes (ML: 5.3-5.5) earthquakes occurred in the Midnapur district of West Bengal (Chandra 1977). The fault plane solutions of these three earthquakes revealed a strike-slip motion along a preferred ENE -WSW trending fault plane with an N-S oriented maximum compression. In 1995, two moderate earthquakes of ML 5.0 took place in the Bonaigarh region near the EGMB (Eastern Ghat Mobile Belt)-Singhbhum craton contact zone (Gupta et al. 2014). Available historical seismicity data suggest that this area had also experienced two or more earthquakes of ML 5.2 in 1958, and 1962, respectively, and two earthquakes of magnitudes ML 4.4 and 4.1 occurred in January 1986 (Gupta et al. 2014). In 1993, one earthquake of ML 4.3 had also occurred in the region south of the NOBF (North Orissa Boundary Fault), or Sukhinda thrust (Fig.1). Additionally, 26 smaller earthquakes (M<3.0) were reported by the Geological Survey of India (GSI) through a temporary microearthquake (MEQ) monitoring in the Bonaigarh-Talchir area during January to mid-May, 1997. Further, recently 160 smaller events, which have occurred in the Dhanbad, Jharkhand, and its surroundings areas during 2007-08, were reported by the Indian School of Mines single station observatory

(Khan et al. 2011). Moment tensor solutions of two local earthquakes of M<3.0, which occurred in the surrounding regions of Dhanbad, Jharkhand, suggested a left-lateral strike slip faulting at 26 km depth (Kayal et al. 2009) (Fig.1). Thus, it can be inferred from the above observations that the strike-slip sense of motion is the dominant deformation mode in our study area.

SEISMIC NETWORK AND EARTHQUAKE DATA

In 2013, a seismic network consisting of fifteen three-component broadband seismographs was installed by the CSIR-NGRI, Hyderabad, in the Singhbhum craton, Chotanagpur plateau and surrounding regions (Fig.1). This temporary seismograph network was established under a twelfth five-year research project scheme of the CSIR-NGRI (Council of Scientific and Industrial Research-National Geophysical Research Institute). The stations are installed on the hard rock site so that signal to noise ratio become high. The recordings of seismographs are done at 50 samples per second at a high gain. Many regional and teleseismic events are recorded by this network during 2103-14. However, local events are much less in the area. Eighteen local events have been identified during 2013-14 and are located using both single station and multiple station method. Out of eighteen events, ten events have been located using multiple station methods and remaining eight events, which were recorded in less than three stations, have been located using single station method. These methods are inbuilt in the SEISAN software (Havskov and Ottemoller 2003).

Earthquake locations for ten local events, which were recorded at 3 or more stations, are obtained using the location program inbuilt in SEISAN software (Havaskov and Ottemoller 2003). Five different 1-D velocity models have been used for locating and calculating moment tensor of local earthquakes. These five models have been shown in Table 1. Model 1 is the modified average one-dimensional crustal velocity model of Kayal et al. (2009), and other four models have been taken from the result of receiver function analysis (Mandal and Biswas, 2016). These local earthquakes are located using five different velocity models as discussed above. After locating these local events, we selected the best hypocentral parameters for these events based on r.m.s, erh and erz values as obtained using five different velocity models as discussed above. Using these better estimated hypocentral parameters, we estimate the source parameters and moment tensors. For moment tensor study, we used model 2 for KEN and KHU stations, and model 3 for HAZ and DMK stations while we used model 4 for SAL and BLS sites, and model 5 for BAL, KNJ, CHI, and DEN sites (Fig.1 and Table 1). Estimated hypocentral and source parameters for selected events are listed in Table 2 and 3, respectively.

METHODOLOGY

Estimation of Earthquake Source Parameters

First, we compute the three component S-wave spectra of each station using SAC (Seismic Analysis Code) where no correction for the Q is applied, but instrumental correction is made using pole-zero files. Next, these spectra are used as input data for Fletcher's simultaneous inversion technique for estimating earthquake source parameters and crustal Q values (Fletcher 1995). However, the Lavenberg–Marquardt inversion method was used instead of singular value decomposition technique used by Fletcher (1995).

The Levenberg–Marquardt algorithm combines beneficial aspects of Gauss-Newton and steepest descent methods, which facilitates the faster convergence of the solution. In this method, first we select the initial values for corner frequency and long period spectral level from the respective spectra and the modeled spectra, i.e., the initial corner frequency is taken by matching the observed spectra and modeled spectra. Next, these initial values are used to calculate the inverted spectra using the ω-square source spectral model. Then, a normalized difference between inverted and observed spectra is calculated. The iteration continues until this difference converges to a minimum value, which gives a better visual fit between observed and inverted displacement spectra that provides us the required model parameters, i.e., corner frequency, long-period spectral level and crustal Q values. Finally, using these model parameters, we calculate the other source parameters like source radius, static stress drop, seismic moment and moment magnitude, using some well-known relations as described in the Saha et al. (2012) and Kumar et al. (2015).

Following the mathematical formulation of Saha et al. (2012) and Kumar et al. (2015), we can write the final equation related to inversion of S-wave spectra (A(f)) as,

$$\ln A(f) = \ln \Pi_0 - 0.5 \ln B_4 + 2B_4^{-1}(f/f_c)^4(\Delta f_c/f_c) - \omega t^*/2 \quad (1)$$

where, Π_0 marks the flat long period spectral level. 'R' term is dropped because the formula for the moment is corrected from the geometrical spreading eûect. Here, $t^* = (R/Q_0V_s)$ and V_s is S-wave velocity (constant). And, B_4 equals to $[(1+f/f_c)^4]^{0.5}$. Here, f and f_c represent frequency and corner frequency, respectively.

Using the concept of least-squares algorithm, the equation (1) can be written as:

$$D = GM \quad (2)$$

The model parameter matrix M, sensitivity matrix G and data matrix D are

$$M = [\ln \Pi_0, t^*, \Delta f_c]^T$$

$$G = [1, -w/2, 2B_4^{-1}(f/f_c)^4 /f_c]$$

$$D = \ln A(f) + 0.5 \ln B_4] \quad (3)$$

Using Newton's method for quasi-linear equation

$$\Delta M = (G^TG)^{-1} G^T\Delta D \quad (4)$$

Where, ΔM is the change in model parameters and ΔD is the difference between predicted data and observed data. The solution is found iteratively $M_k = M_o + M_{k-1}$ where M_o is the initial model. As the sensitivity matrix is near to singular here, thus, we use the Lavenberg-Marquardt inversion technique to estimate $\ln\Pi_o$, t^* and f_c with ten iterations. In this technique, the equation (9) can be written as:

$$\Delta M = (G^TG + \lambda I)^{-1} G^T\Delta D \quad (5)$$

Where, λ is Levenberg–Marquardt adjustable damping parameter

Table 1. Velocity models used for earthquake location and moment tensor inversion studies

Model 1		Model 2		Model 3		Model 4		Model 5	
Depth (km)	Velocity (km/s)	Depth (km)	Velocity (km/s)	Depth (km)	Velocity (km/s)	Depth (km)	Velocity (km/s)	Depth (km)	Velocity (km/s)
0.0	5.62	0.0	5.72	0.0	5.38	0.0	5.87	0.0	5.91
4.0	5.72	4.8	6.36	4.8	6.07	5.1	6.55	5.25	6.27
8.0	5.79	19.6	6.85	25.0	6.62	25.1	6.93	15.25	6.60
12.0	5.87	39.0	8.00	40.0	8.00	46.0	8.04	25.4	6.87
15.3	6.61							42.8	8.00
40.1	8.14								

Table 2. Estimated hypocentral parameters for selected ten earthquakes, which are located using multiple stations (e" 4 stations)], from the Eastern Indian Shield

Event no	yymmdd	Origin Time hh:mm:ss	Latitude (degree)	Longitude (degree)	Depth (km)	Mw
1	20130208	10:54:44.67	21.01	86.32	16.9	3.01
2	20130215	23:56:15.86	20.81	85.65	18.0	2.51
3	20130220	05:14:07.41	20.99	85.17	9.7	3.01
4	20130316	19:42:10.20	22.92	87.43	9.0	3.04
5	20130519	08:27:35.21	23.65	85.07	34	2.44
6	20130521	06:06:34.92	22.04	86.92	12.6	2.64
7	20130601	13:27:57.21	21.96	88.35	15	3.57
8	20130605	18:40:11.04	20.53	85.87	21.6	3.12
9	20130910	17:43:51.91	23.85	86.18	14.6	2.95
10	20130910	18:06:16.67	23.86	86.18	18.9	2.50

and I is the identity matrix. The Levenberg–Marquardt method is selected because (i) it combines beneficial aspects of Gauss–Newton and gradient methods while avoiding some of their weaknesses, (ii) the solution converges quickly, and (iii) in many cases a standard guess works well. In this study, λ value varies from 1 to 100.

The inversion begins with the initially guessed value of the model parameter (M) i.e. corner frequency f_c, t* and spectral level Π_o. The initial guessed value of Δf_c was set at 0.1 Hz for all events, while that of Π_o was selected visually from the respective low-frequency spectral level. And, the initially guessed value of t* is calculated using the equation $t^*=R/Q_oV_s$, where R is the hypocentral distance (in km). And for the Singhbhum region, Q_o is considered as 508 (Singh et al. 2004) while V_s is assumed to be 3.5 km/s. For every iteration, the normalized difference between the computed spectra obtained from the theoretical formula and that yielded from equation (5) is computed. The maximum and minimum expected values of such difference are pre-set at the start of the iteration. The maximum difference is selected from the initially guessed values of Π_o, t* and f_c, and the minimum value is set based on the accuracy of Π_o, t* and f_c values that one can expect to obtain from the inversion of noisy data. We also assign an initial value to ë, say 0.001. By substituting these initial guessed values into equation (5), the change in model parameter vector, ΔM, is derived. In the next iterations, a new model parameter is computed according to $M_{r+1} = M_r + \Delta M_r$, where M_r and ΔM_r are the model parameters and change in parameter values at the r^{th} iteration.

After obtaining model parameters from the above-mentioned inversion technique, source parameters such as seismic moment (in N-m), source radius (in m), stress drop (in MPa), moment magnitude, radiated seismic energy (E_R, in Joule), radiated S-wave energy (E_S, in Joule), apparent stress (in MPa) and Zuniga parameters are estimated using some empirical equations as given in Kumar et al. (2015), Abercrombie and Rice (2005), Zuniga (1993) and Singh and Ordaz (1994). Other parameters used for computing source parameters are discussed in the following. 'V_S' and 'ρ' are the S-wave velocity in m/s and rock density in kg/m^3 at the source, respectively. Here 'ρ' is calculated from V_P [= $(0.32V_P + 0.77)$, where V_P is the P-wave velocity in m/s (Berteusen 1977)]. And, Π_i and f_i mark the long-period spectral level (in m-s) and corner frequency (in Hz) for corresponding three component digital seismograms, respectively. 'R' is the hypocentral distance in m, while 'F' represents the free surface amplification factor, which is assumed to be 2. $R_{\varphi\phi}$ is the average radiation pattern, (0.55; Singh et al. 2003). We take $Q(f) = 508\ f^{0.48}$, which is taken according to Singh et al. (2004) for attenuation factor for Indian shield. F_S is the free surface effect (=2) while β is S-wave velocity (~3500 m/s). And, ρ is the density (~2700 kg/m^3). To estimate apparent stress, rigidity modulus (μ) from the P-wave and S-wave velocity structure of the Singhbum craton was calculated.

For Orowan's model, *Zuniga parameter* (ε_z) = 1 and $\sigma_2 = \sigma_f$. Thus, apparent stress equals to half of the static stress drop i.e., $\sigma_a = [\Delta\sigma/2]$ (Savage and Wood, 1991). The σ_1 and σ_2 are initial and final average stresses while σ_f is the average stress during faulting. Now, for overshoot model final average stress becomes less than average stress during faulting i.e. $\sigma_2 < \sigma_f$ (i.e., $\sigma_a < [\Delta\sigma/2]$) while for partial stress drop model $\sigma_2 > \sigma_f$ (i.e., $\sigma_a > [\Delta\sigma/2]$). Also, it can be written that the case $\varepsilon_z < 1$ represents the partial stress drop model while $\varepsilon_z > 1$ describes the overshoot model.

Following the methodology of Archuleta et al. (1982), the error in the source parameters was analyzed by estimating the standard deviation and mean of the moment (M_0), source radius (r), and stress drop. The details of error analysis of source parameters can be found in Kumar et al. (2015).

Moment Tensor Inversion

The moment tensor (MT) inversion for multiple point sources is performed using the ISOLA software (Sokos and Zahradnik 2008), which uses the iterative deconvolution technique of Kikuchi and Kanamori (1991) for inversion of complete regional and local waveforms (Sokos et. al. 2013). In this method, the full wavefield synthetics (i.e. Green's functions at local and regional distances) are computed using the discrete wavenumber method of Bouchon (1981) and Coutant (1989). Initially, a set of predefined point-source positions along a line or on a plane is considered. After obtaining a major point-source contribution or sub-event, the corresponding synthetics are subtracted from data. Then, the residual waveform is inverted for another point source, and so on (Zahradnik et al. 2005). Here, the point sources are removed consecutively, one after another, thus, each step involves only two parameters (source position and onset time), which provides stability of the inversion (Zahradnik et al. 2005). To get the best position and onset time, a grid search method is used that provides the best position and time in terms of the absolute value of the correlation coefficient between the observed and synthetics. The correlation coefficients are calculated automatically during least squares inversion (Dimri, 1992; Zahradnik et al. 2005). At the best-fitting spatiotemporal position, the match between the observed and

Table 3. Estimated source parameters and crustal Q values for selected ten earthquakes from the Eastern Indian shield

Event No.	f_c Hz	s. d. (f_c)	R (m)	s. d. (R)	M_0 (N-m)	Δσ MPa	s. d. <Δσ>	$\Delta\sigma_a$ (MPa	Em_0	Q_0	E_S (Joules)	E_R (Joules)
1	7.60	0.25	171.8	5.09	4.4E+13	0.46	0.20	0.94	1.63	3397	1.5E+09	3.5E+08
2	8.50	0.32	144.2	5.03	7.4E+12	0.11	0.03	0.10	1.44	1164	3.0E+07	1.3E+07
3	7.56	0.70	173.7	15.5	4.6E+13	0.46	0.21	0.62	1.77	3852	9.9E+08	3.7E+08
4	7.64	0.04	152.4	0.72	4.7E+13	0.58	0.17	0.46	1.33	2735	5.3E+08	4.2E+08
5	8.62	0.30	157.6	5.10	6.2E+12	0.08	0.04	0.10	1.76	1176	1.9E+07	8.5E+06
6	8.37	0.09	152.0	1.53	1.3E+13	0.17	0.12	0.08	2.13	1091	3.1E+07	4.3E+07
7	6.23	0.37	211.3	11.2	7.1E+14	4.13	1.34	0.78	2.16	4926	2.0E+10	5.1E+10
8	7.27	0.34	163.5	6.89	6.3E+13	0.62	0.20	0.23	1.46	3353	2.5E+08	6.4E+08
9	8.31	0.20	154.9	3.61	3.8E+13	0.44	0.28	0.47	1.89	4240	4.9E+08	3.3E+08
10	8.62	0.39	144.5	6.38	7.4E+12	0.11	0.04	0.06	1.59	4127	8.3E+06	1.3E+07

synthetics data is characterized by the overall variance reduction (over all stations and components) (Zahradnik et al. 2005). The remaining part (i.e. the deviatoric moment tensor inversion) is linear, which calculates only five-moment tensor components. An L2 norm least squares inversion is used to obtain the moment tensors of the subevents by minimizing the difference between observed and synthetic displacements, whose moment rate has a predefined shape and duration. In our modeling, a delta function is used.

In this paper, the deviatoric moment tensor inversion available in the ISOLA-GUI package is used (Sokos and Zahradnik, 2008 and 2013). The constraint is nonlinear, which is applied iteratively using the method of Lagrange multipliers. The details of the technique can be found in Zahradnik et al. (2005). Velocity records in SAC format as input data for moment tensor inversion was used. The data is processed in different steps by using the software like band-passed (here 0.05-1.5 Hz) filtering, cosine tapering (5%), origin alignment, etc. ISOLA integrates the input data to the band-passed displacement, which are then used as input for the moment tensor inversion. A four band passed filter (f_1, f_2, f_3, f_4), which is applied both to real and synthetic waveforms, is flat (=1) between f_2 and f_3, and cosine-tapered between f_1 and f_2, and again between f_3 and f_4. The SNR curves help mainly to define f_1 because the noise level (either natural or instrumental) limits the usable low-frequency range (Sokos and Zahradnik 2013). The f_4 value is dictated by knowledge of the earth structure. With existing crustal models, near stations (<~100 km) can be inverted up to ~1 Hz, whereas near-regional stations (~100 km) can be inverted up to <0.1 Hz, and regional stations ~1000 km up to ~0.01 Hz (Sokos and Zahradnik, 2013). In this paper, station dependent frequency range is used according to the SN (signal-to-noise) ratio and the epicentral distance, which is described in the results section.

RESULTS

Source parameters of ten local events (Table 3) are estimated by inverting the S-wave displacement spectra from three-component broadband recordings from 3-6 stations in the EIC, wherein, an iterative Levenberg-Marquardt inversion technique is used. The estimated seismic moment (M_0) and source radius (r) vary from 7.4 x 10^{12} to 7.1 x 10^{14} N-m and 144.2 to 211.3 m, respectively, while estimated stress drops ("ó) and multiplicative factor (E_{mo}) values range from 0.11 to 1.43 MPa and 1.33 to 2.16, respectively (Figs. 2a and b; Table 3). The corner frequencies are found to be ranging from 6.23 to 8.62 Hz while moment magnitudes are varying from 2.44 to 3.57 (Fig.2a). The plot between seismic moment and source radius (Fig.2b) suggests no break in self-similar source scaling but suggests a much higher slope

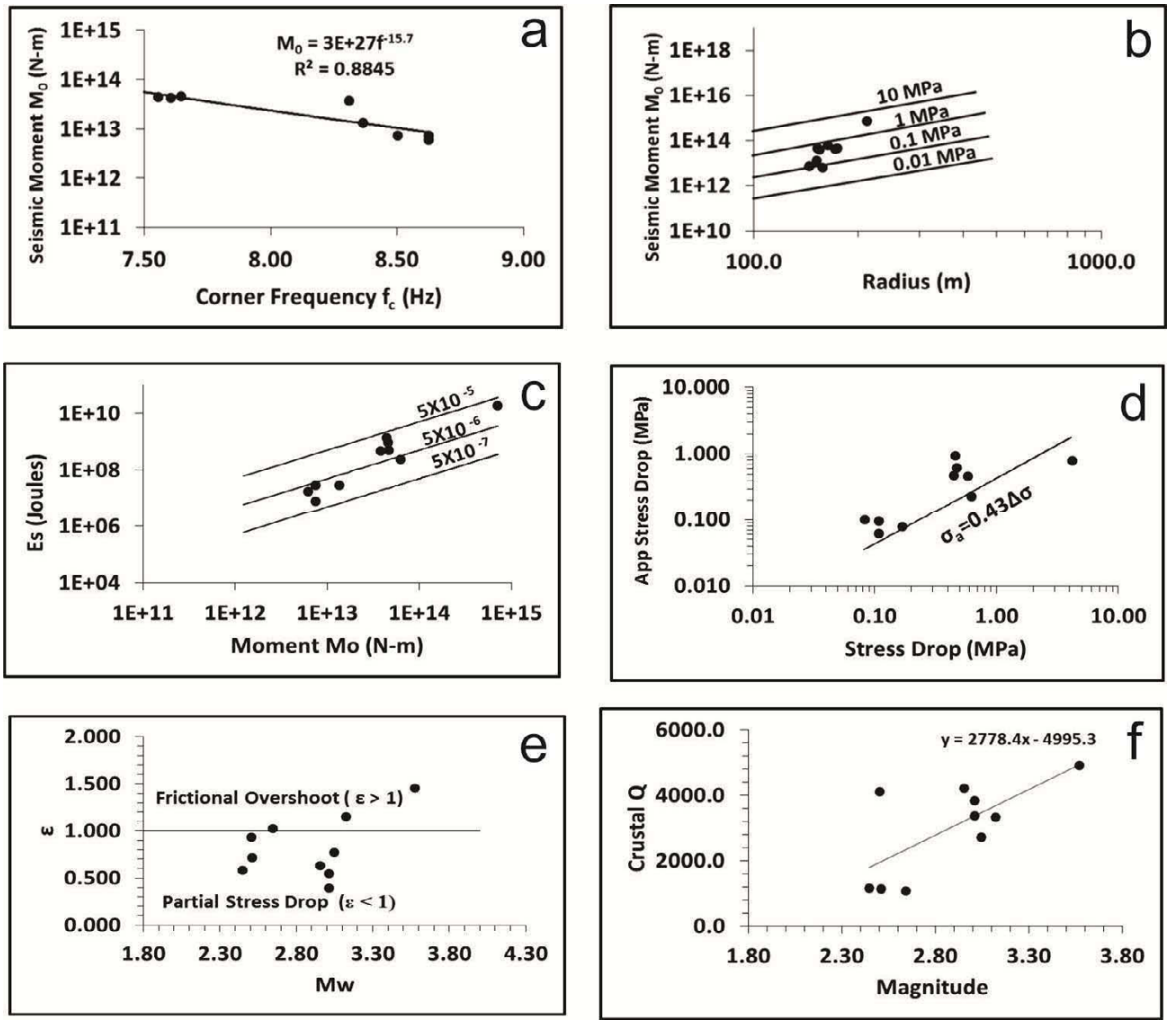

Fig.2. (a) Plot between corner frequency (fc in Hz) and seismic moment (M_0 in N m) showing no break in linear scaling, (b) Log–log plot between source radii (r in m) and seismic moment (M_0 in N m) showing no break in source scaling, (c)Seismic energy (Es) and seismic moment (M_0) for selected 10 local earthquakes, with black solid lines of constant e values of 5 x 10^{-4}, 5 x $10^{-5}$and 5 x 10^{-6}, (d)Variation in estimated apparent stress values with static stress drops showing theoretical relation in black line, (e) A plot showing variation in Zuniga (å) parameter with moment magnitudes for selected 10 Eastern Indian peninsular local earthquakes. Black solid line at å = 1 separates the events with frictional overshoot (å>1) and partial stress drop (å<1) mechanisms, and (f) A plot showing crustal Q variation with Mw.

than linear scaling (i.e. $M_o \infty f_c^{-3}$). Figure 2d showed a variation in apparent stresses (σ_a) with Brune(1970)'s static stress drop (Ds) estimates, wherein the relation $\Delta\sigma = 0.43\ \sigma_a$ (Singh and Ordaz 1994) is also shown. Our apparent stress estimates are found to be lower than static stress drops for all the selected Singhbhum earthquakes. We notice that the estimated stress drop for a Singhbhum cratonic event of M_w3.57 is found to be larger in comparison to that of the same size event from other tectonic regions of India. Estimated Zuniga parameters suggest that all the selected events satisfy the Partial Stress Drop model, which is in agreement with the global observations (Fig.2e). The radiated seismic energy and apparent stresses range from 8.3×10^6 to 2.0×10^{10} Joules and 0.06 to 0.94 MPa, respectively (Fig.2c).The crustal S-wave quality factor varies from 1091 to 4926 with an average of 3006 for the study region (Fig.2f).

The deviatoric moment tensor inversion for multiple sources (source below the epicenter) is performed, using ISOLA software, on the displacement traces obtained from the broadband data of five selected small earthquakes from the eastern part of Indian peninsula. The moment magnitude (M_w) is ranging from 3 to 3.57. The good agreement between observed traces and synthetics are shown in (Figs. 3a, 4a, 5a, 6a, and 7a). As the seismological network has been deployed mainly for studying the crustal and lithospheric structure of the area by using regional and teleseismic earthquakes, thus, sufficient stations are not available to study the moment tensor solutions of local earthquakes. So, out of five events, we have used two stations for four events, four stations for one event to calculate the moment tensor solutions using ISOLA software. The event-wise result of deviatoric multiple sources MT inversion is discussed below.

Event 1 (08.02.2013, 10:54)

This M_w3.0 event occurred at the location of latitude 21.03°N and longitude 86.31°E. For this event, 3-component broadband waveforms from two stations [Keonjhar (KNJ) and Denkanal (DEN)] are used. In this case, the velocity model 5 is used for green function computation (Table 1). The epicentral distances for KNJ and DNK are 28 and 111 km, respectively. The band-pass frequency is used in the range of 0.07 to 0.11 and 0.13 to 0.15 Hz. The initial frequency is selected by signal to noise ratio (Fig.3c). A set of predefined 40 point-source positions at every 1 km depth beneath the epicenter starting from 5 to 45 km is considered. The deviatoric MT inversion provides the maximum spatial correlation at 40 km depth (Fig.3b), suggesting a solution having 61.5% of DC component and 38.5% of CLVD component (Fig. 3b and Table 4). The mechanism suggests a left-lateral strike slip movement (rake 15) along a northwest trending steeply (~55°) dipping fault (Fig.1). The P-axis orientation is estimated to be 350° (Table 4) for this event indicating the maximum compression acting in the NW-SE direction.

Event 2 (20.02.2013, 05:15)

This M_w3.01 event occurred at the location of latitude 20.99°N and longitude 85.17°E. For this event, 3-component broadband waveforms from two stations [Denkanal (DEN), Khurda (KHU)] are used. In this case, the velocity model 2 and five are being used for green function computation for KHU and DEN, respectively (Table 1). The epicentral distances for DEN and KHU are 11 and 98 km, respectively. The band-pass frequency is used in the range of 0.06 to 0.08 and 0.1 to 0.12 Hz. The initial frequency is selected by signal to noise ratio (Fig.4c). A set of predefined 20 point-source position at every 1 km depth beneath the epicenter starting from 5 km to 25 km is considered. The deviatoric MT inversion provides the maximum spatial correlation (~0.9) at 17 km depth, suggesting a solution having 98.3% of DC component and 1.7% of CLVD component (Fig. 4b and Table 4). The centroid depth is found to be 17 km. The mechanism suggests a dextral strike-slip movement with a small normal component (rake -2°) along a northwest trending steeply (~63°) dipping fault (Fig.1). The P-axis orientation is estimated to be 176° (Table 4) for this event suggesting the maximum compression acting in the N-S direction.

Event 3 (16.04.2013, 03:05)

This M_w3.06 event occurred at the location of latitude 21.87°N and longitude 86.42°E. For this event, 3-component broadband waveforms from two stations [Salbani (SAL) and Bhubaneswar (BHN)] are used. In this case, velocity model 4 and two are being used for green function computation of SAL and BHN, respectively (Table 1). The epicentral distances for SAL and BHN are 42 and 134 km, respectively. The band-pass frequency is used in the range of 0.07 to 0.1 and 0.12 to 0.14 Hz. A set of predefined 40 point-source position at every 2 km depth beneath the epicenter starting from 5 km to 45 km is considered. The deviatoric MT inversion provides the maximum spatial correlation (~0.68) at 23 km depth (Fig.5b), suggesting a solution having 92.0% of DC component and 8.0% of CLVD component (Fig.5b and Table 4). The centroid depth is found to be 23 km (Fig.5b). The mechanism suggests a left lateral strike slip motion with a minor normal component (rake -168°) along a northwest trending shallow (~20°) dipping fault (Fig.1). The P-axis orientation is estimated to be 31° (Table 4) for this event that reveals the maximum compression acting in the NE-SW direction.

Event 4 (01.06.2013, 13:28)

This M_w3.57 event occurred at the location of latitude 21.96°N and longitude 88.35°E. For this event, 3-component broadband waveforms from two stations [Balukuria (BAL) and Keonjhar (KNJ)] are used. In this case, velocity model 5 is used for green function computation (Table 1). The epicentral distances for BAL and KNJ are 161 and 225 km, respectively. For BAL station, the band-pass frequency is used in the range of 0.06 to 0.08 and 0.10 to 0.12 Hz. A set of predefined 10 point-source position at every 2 km depth beneath the epicenter starting from 2 km to 20 km is considered. The deviatoric MT inversion provides the maximum spatial correlation (~0.7) at 8 km depth, suggesting a solution having 87.9% of DC component and

Table 4. Strike, dip, rake, CLVD%, DC%, P-axis, T-axis, azimuth and trend as obtained from moment tensor inversion of five selected events.

S. No	DDMMYY	DC (%)	CLVD (%)	Strike (°)		Dip (°)	Rake (°)	P-axis		T-axis	
								Az.	Pl.	Az.	Pl.
1	08-02-2013	61.5	38.5	NP:1	35	55	15	350	15	250	33
				NP:2	297	78	144				
2	20-02-2013	98.3	1.7	NP:1	218	63	-2	176	20	80	17
				NP:2	309	88	-153				
3	16-04-2013	92	8	NP:1	203	20	-168	31	46	174	38
				NP:2	101	86	-71				
4	01-06-2013	87.9	12.1	NP:1	278	71	-69	217	58	352	24
				NP:2	48	28	-137				
5	10-09-2013	74	26	NP:1	225	23	-116	360	64	155	24
				NP:2	73	70	-80				

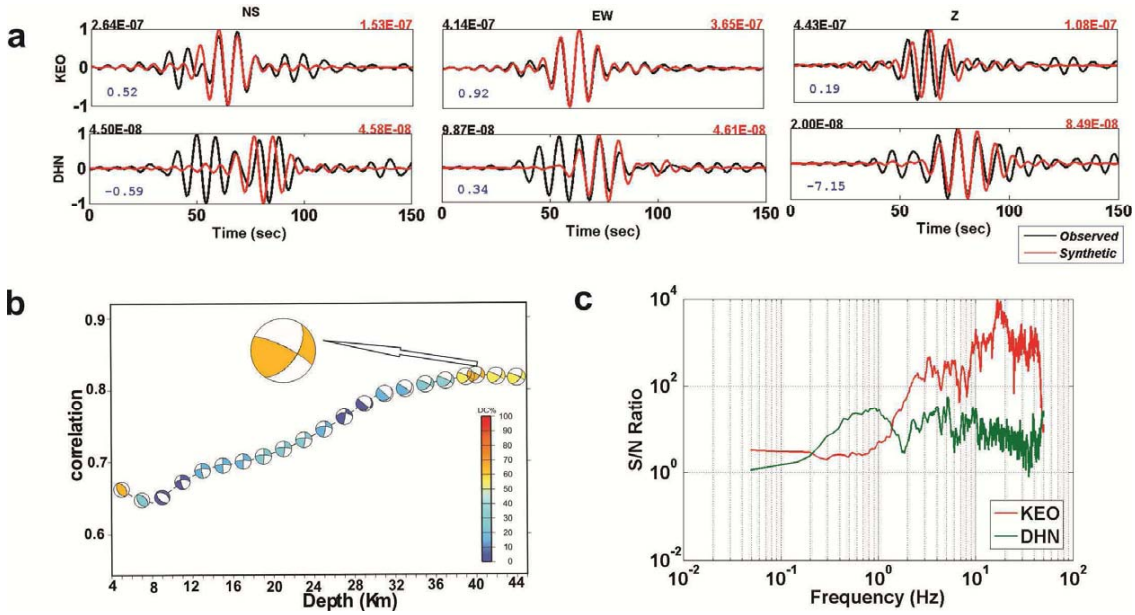

Fig.3. Solutions of MT inversion for event 1 (08.02.2013 10:54) **(a)** A plot Showing Synthetic and observed traces, **(b)** A plot Showing correlation versus depth, and **(c)** A plot showing signal-to-noise ratio versus frequency, the initial frequency for inversion is fixed according to this.

12.1% of CLVD component (Fig.6b and Table 4). The centroid depth is found to be 8 km (Fig.6b). The mechanism suggests a normal dip-slip motion with a minor strike-slip component (rake -69°) along a northeast trending steeply (~71°) dipping fault (Fig.1). The P-axis orientation is estimated to be 217° (Table 4) for this event, which depicts the maximum compression acting in the NE-SW direction.

Event 5 (10.09.2013, 17:43)

This M_w2.95 event occurred at the location of latitude 23.48°N and longitude 86.18°E. For this event, 3-component broadband waveforms from four stations [Nirsa (NIR), Hazaribagh (HAZ), Ranchi (RAN) and Lohardaga (LOH)] are used. In this case, velocity model 3 is used for green function computation (Table 1). The epicentral distances for NIR, HAZ, RAN and LOH are 50, 85, 96 and 165 km, respectively. The band-pass taper frequency for all four stations is used in the range of 0.07 to 0.09 and 0.10 to 0.12 Hz. A set of predefined 45 point-source position at every 2 km depth beneath the epicenter starting from 5 km to 50 km is considered. The deviatoric MT inversion provides the maximum spatial correlation (~0.8) at 40 km depth (Fig.7b), suggesting a solution having 74.0% of DC component and

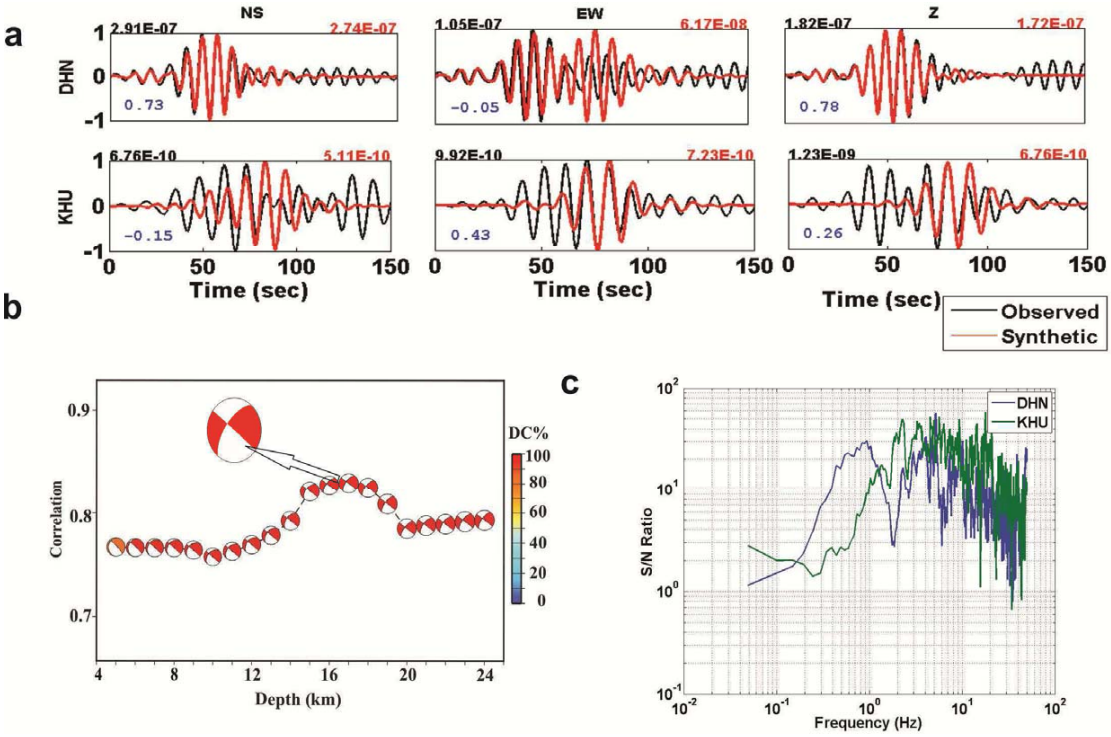

Fig.4. Solutions of MT inversion for event 1 (20.02.2013 05:15) **(a)** A plot Showing Synthetic and observed traces, **(b)** A plot Showing correlation versus depth, and **(c)** A plot showing signal-to-noise ratio versus frequency, the initial frequency for inversion is fixed according to this.

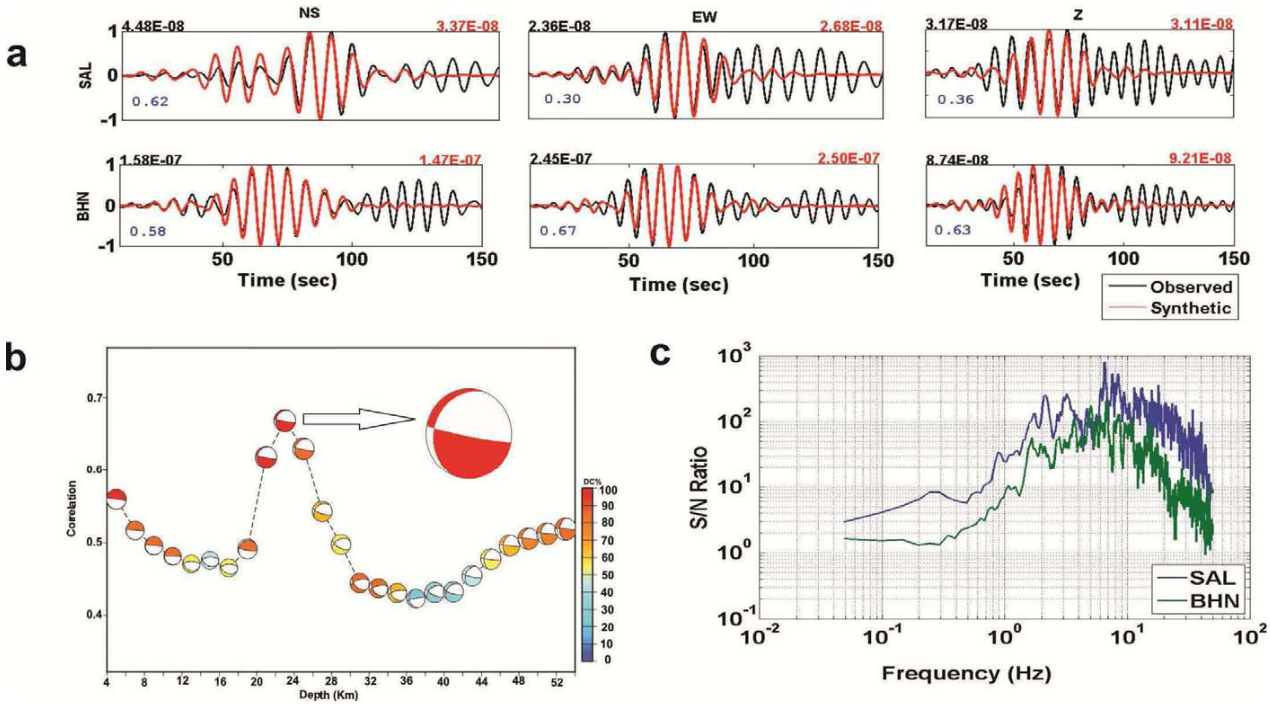

Fig.5. Solutions of MT inversion for event 1 (16.04.2013 03:05) **(a)** A plot showing synthetic and observed traces, **(b)** A plot showing correlation versus depth, and **(c)** A plot showing signal-to-noise ratio versus frequency, the initial frequency for inversion is fixed according to this.

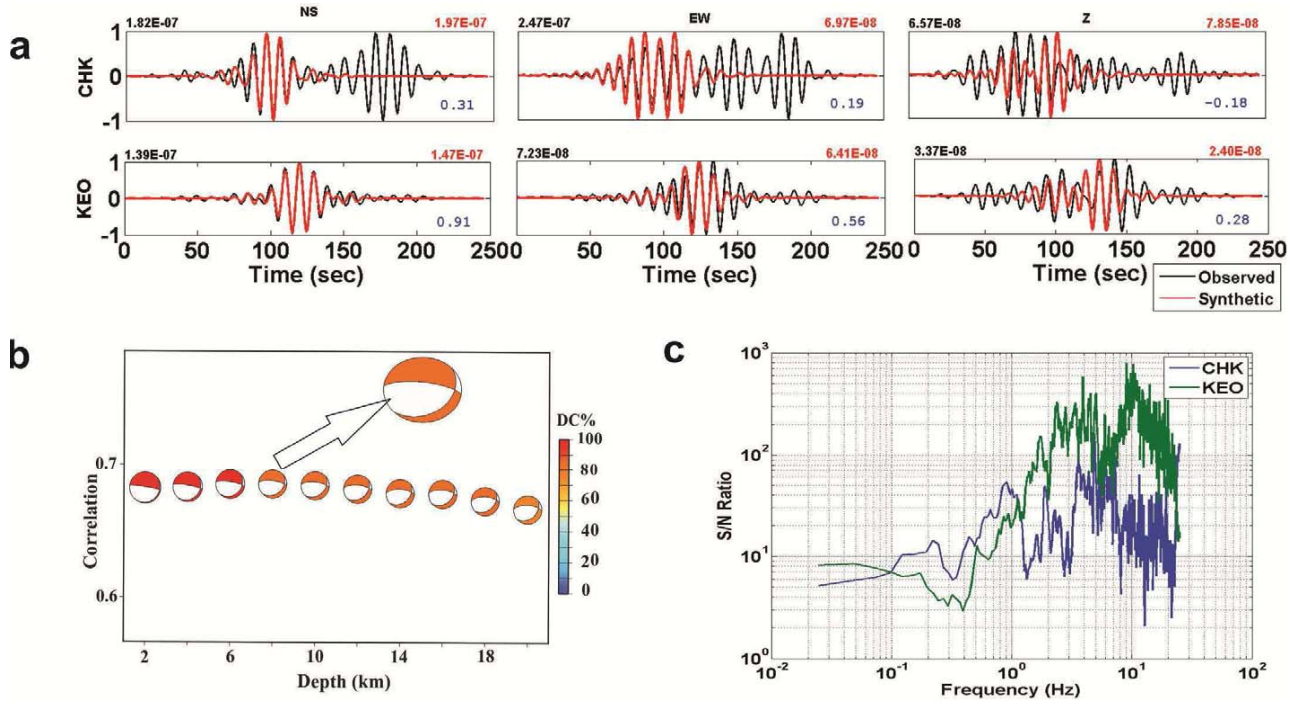

Fig.6. Solutions of MT inversion for event 1 (01.06.2013 13:28) **(a)** A plot Showing Synthetic and observed traces, **(b)** A plot Showing correlation versus depth, and **(c)** A plot showing signal-to-noise ratio versus frequency, the initial frequency for inversion is fixed according to this.

26.0% of CLVD component (Fig.7b and Table 4). The centroid depth is found to be 40 km (Fig.7b). The mechanism suggests a normal dip-slip motion with a minor strike-slip component (rake -116°) along a southeast trending shallow (23°) dipping fault (Fig.1). The P-axis orientation is estimated to be 360° (Table 4) for this event, which suggests the maximum compression acting in the N-S direction.

DISCUSSION AND CONCLUSION

We have investigated source processes involved in generating earthquakes occurring in the eastern Indian shield, through the estimation of source parameters and moment tensors of local earthquakes of M_w2.44-3.57, which have occurred during 2013-14. One of the findings of this study is that the estimated source parameters are showing an apparent deviation from the self-similarity as suggested by Kanamori and Anderson (1975) and Hanks (1977). This model receives further support from the fact that the plot of the estimated corner frequencies (f_c, in Hz) with seismic moments (M_o, in N-m) in log-log scale satisfies the relation $M_o \infty f_c^{-(3+\varepsilon)}$ for ε= 12.7 (Fig.2a),

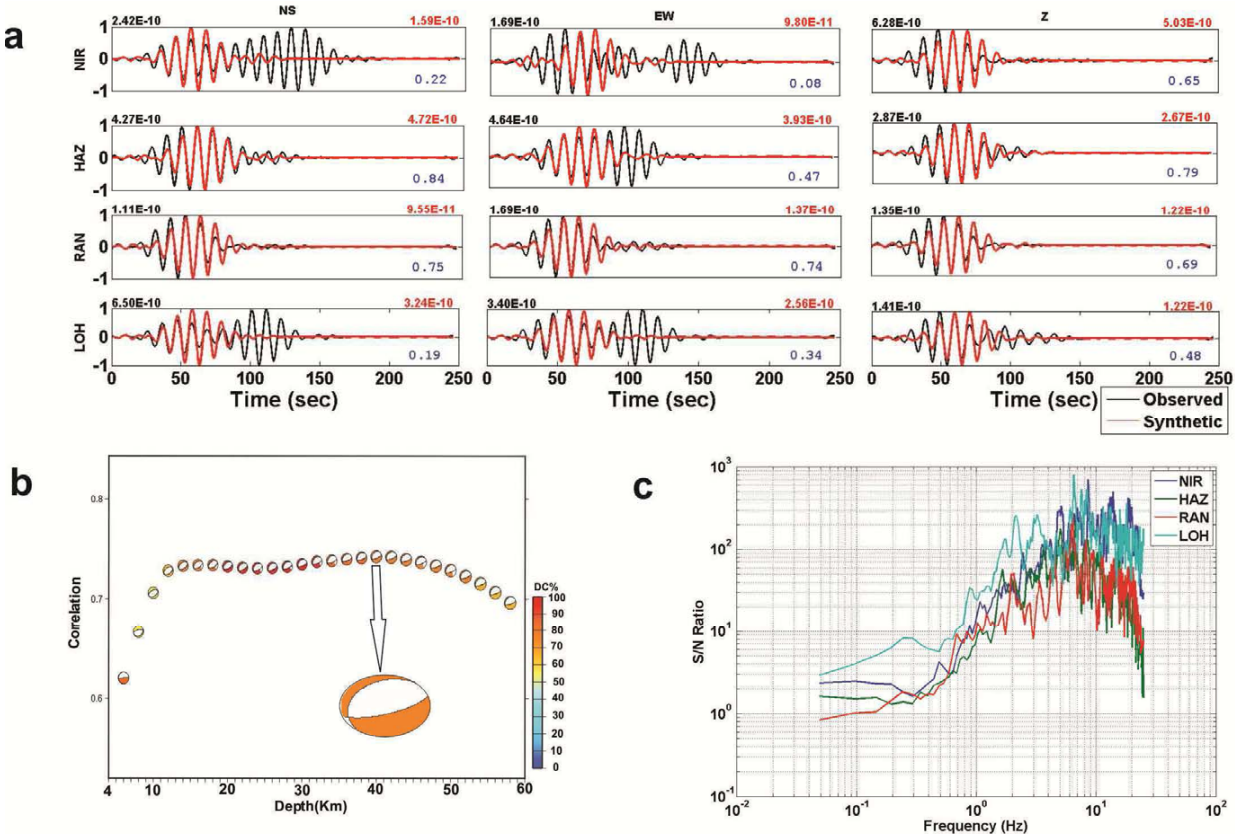

Fig.7. Solutions of MT inversion for event 1 (10.09.2013 17:43) **(a)** A plot Showing Synthetic and observed traces, **(b)** A plot showing correlation versus depth, and **(c)** A plot showing signal-to-noise ratio versus frequency, the initial frequency for inversion is fixed according to this.

thus, the source scaling of these events perhaps deviates from the self-similarity i.e. f^{-3}. These inferences are based on only ten events. Thus, we are not very sure about the non-self-similar nature of the source scaling of these cratonic earthquakes. However, the modeling of source parameters of ten local earthquakes supports the non-self-similar scaling. Since the available magnitude range for the selected events varies from 2.44 to 3.57, thus, the study of earthquake scaling for smaller and larger events is beyond the scope of the present investigation. Due to the above fact, estimated source radius and seismic moment apparently suggest no break in self-similar source scaling (Fig.2b). Figure 2c shows the plot of total seismic energy versus seismic moment along with the lines of constant E_s/M_o values. This suggests that the energy may vary from a given seismic moment. The apparent stress estimates are found to be lower than static stress drops for all the selected Singhbhum earthquakes (Fig.2d). The estimated Zuniga's (1993) parameter (e_z) based on apparent stress and static stress drop estimates suggests a partial stress drop mechanisms for these selected local earthquakes in the eastern Indian shield (Fig.2e), which is in agreement with the global observations (Zuniga, 1993). The estimated scaled energy (~E_s/M_o) ranges between 10^{-5} and 10^{-7} (Fig.2c). In general, it is observed that E_s/M_o varies from $5x10^{-4}$ to $5x10^{-6}$ for earthquakes around the world (Singh and Ordaz, 1995). Thus, it can be noted from Fig.2e that some of the estimates agree with global observations, which could be related to the problem in estimating radiated energy for smaller earthquakes. The estimated crustal S-wave quality factor varies from 1091 to 4926 with an average of 3006 for the study region (Fig.2f), suggesting a less heterogeneous crustal structure underlying the eastern part of the Indian shield in comparison to that of the western and northern parts of the Indian shield (Mandal et al., 2004; Mohanty et al., 2009).

The result of moment tensor solutions of selected five local events is shown in Table 4 and Fig.1. The MT solution of 20.02.2013 event of M_w3.0 suggests a pure left-lateral S-S motion on the Sukhiunda thrust. And it can be inferred that the Sukhiunda thrust is presently behaving as a left-lateral S-S fault. Another M_w3.1 earthquake of 16.04.2013 took place in the Singhbum granite region, whose MT solution also reveals a left-lateral S-S motion. In Chotanagpur plateau, one event of magnitude 3.0 occurred on 10.09.2013 in a region near to Dhanbad. The MT solutions of this earthquake suggests a normal dip-slip motion along a south dipping plane. On 01.06.2013, another event occurred in the region of Quaternary sediments lying east of the study area (Fig.1). The MT solution of this event of M_w3.6 reveals a normal dip-slip faulting with a minor S-S. Based on above discussion, it can be inferred that the dominant deformation mode for the eastern Indian shield is left-lateral strike slip motion with minor normal dip-slip component on an almost vertical plane suggesting the important role played by the neotectonics (i.e., vertical movement) in generating these local events. Estimated and available focal mechanisms suggest that the seismically mildly active Singhbhum shear zone and Eastern Ghats mobile belt are showing left-lateral strike motion while two events in Gondwana half graben suggest a normal dip-slip motion along a south dipping plane.

Although the east Indian region has a mild seismicity rate on an average, Fig.1 shows moderate concentration in two areas: one in the Singhbhum shear zone and the other in the Chotanagpur half graben including Hazaribagh. It is established that the continental crust in the Singhbhum shear zone was subjected to an extreme degree of cratonization and thickening (Sarkar 1982) while the Chotanagpur half graben is characterized by thick sedimentary sequences (Naqvi and Rodgers, 1987). Figure 1 shows the occurrences of two M5 historical earthquakes in the Singhbhum shear zone while it also suggests the occurrences of two damaging historical earthquakes (M

4.3 and 5.7) in the Hazaribagh shear zone. Further, it is noticed that several small to moderate events have occurred in these shear zones even in the recent times (Figure 1). Further, the occurrence of two M≤3 events in the Ranipather shear zone is noticed. Additionally, four M3 events occurred along the contact between Singhbhum shear zone and Purulia shear zone, and Purulia shear zone and Chotanagpur half graben. Note that no earthquakes have been noticed in the northeastern quadrant of our study area, which is characterized by thin sedimentary layers. This indicates that crustal weaknesses caused by high levels of extension, as well as flexural stresses, are important factors in defining seismicity rates in passive margins (Assumpcao, 1998). The concentration of seismicity in the continental margin is a common pattern of global seismicity as shown by Schulte and Mooney (2005), but local conditions can cause significant variations along the margin, as shown by Sandiford and Egholm (2008) for Australia.

Probable Causes of Seismicity in the Eastern Indian Shield

For the stable cratonic regions, it is natural to test if the present seismicity tends to be close to the mapped neotectonic structures. Figure 1 shows tectonic faults and lineaments as reported by different authors. We now test if the epicenters of the existing earthquake catalog tend to lie close to the proposed tectonic / neotectonic features. Using the available catalog (ML > 3.5), we compared the number of observed epicenters closer than 20 km (or 10 km) to any fault segment, with the expected number assuming a random distribution of events in the continental area of the eastern Indian shield. The criterion of 10 and 20 km distance was used because this is roughly the estimated epicentral accuracy of most events in the catalog.

This is the case of Singhbhum shear zone and Eastern Ghats mobile belt in the south of the study region, where zones of ongoing seismicity are relatively well defined due to many detailed studies of earthquake swarms and aftershocks using local networks. A clear example of the association of present-day seismicity with geological features is the Singhbhum shear zone, reactivated in the brittle crust during the Gondwana breakup in the Cretaceous. A clear association of the seismicity with several small faults in the E-W trending Chotanagpur half graben belt is noticed, which is a neo-tectonically active area (Fig.1). Seismological studies indicated that these zones had been reactivated in the past. However, several other lineaments in the study area do not have any evidence of paleoseismicity, historical or instrumental seismicity. Thus, some earthquakes in the Quaternary zones in the east of study area have no direct correlation with large geological lineaments mapped at the surface, even when the epicenters are apparently very close to a major fault or shear zone.

The explanation for the reactivation of major lineaments, where others remain aseismic, is a matter of debate. For example, in the Eastern Ghats mobile belt and Singhbhum craton, major shear zones were reactivated in the Gondwana breakup, and they form the boundaries of rifts (Behera et al. 2005). The occurrence of pseudotachylyte in these mylonitic belts in the Mahanadi shear zone, the Eastern Ghats mobile belt (Mahapatro et al. 2009) implies that they are exhumed paleoseismic zones. However, other continental – scale E-W trending shear zones in the study area also present a long history of brittle reactivation and are also under the N-S trending maximum compression (SH_{max}) and the E-W trending extension (SH_{min}) such as Singhbhum, Purulia and Ranipathar shear zones, the Eastern Ghats mobile belt and Chotanagpur half-graben belt. A question remains as to why these other shear zones do not show present-day seismicity. Several processes have been proposed to explain mechanical fault weaknesses, such as the occurrence of low friction material (Morrow et al. 1992) or the presence of high fluid pressure in the fault zone (Byerlee 1978; Sibson 1984). However, there is a paucity of evidence to support the idea that some of these processes can be responsible for the weakening of fault zones (Holdsworth et al. 2001). As intraplate fault present long recurrence periods (Rajendran et. al. 2008), it is possible that these continental –scale features present dormant structures. It follows that the short period of instrumental monitoring, poorly known seismicity, and lack of systematic paleoseismic investigations in the Eastern Indian shield indicate that further studies are necessary to address this problem.

Acknowledgements: Authors are grateful to the Director, NGRI, Hyderabad, for his kind permission to publish this work. This study is supported by the Council of Scientific and Industrial Research (CSIR) twelfth five year plan project (Index) at the CSIR-National Geophysical Research Institute, Hyderabad.

References

Abercrombie, R.E. and Rice, J.R. (2005) Small earthquake scaling revisited: can it constrain slip weakening? Geophys. Jour. Internat., v.162, pp.406-424.

Acharya, S. (1984) Stratigraphic and structural evolution of the rocks of the iron ore basins in Singhbhum-Orissa Iron Ore Province, India, CEISM Seminar, Indian Jour. Earth Sci. v.1, pp.19-28.

Acharyya, S.K., Gupta, A. and Orihashi, Y. (2010a) New U-Pb zircon ages from Palaeo-Mesoarchaean TTG gneisses of the Singhbhum Craton, eastern India. Geochemical Jour., v.44, pp.81-88.

Acharyya, S.K., Gupta, A. and Orihashi, Y. (2010b) Neoarchaean-Palaeoproterozoic stratigraphy of the Dhanjori basin, Singhbhum craton, Eastern India: and recording of a few U-Pb zircon dates from its basal part. Jour. Asian Earth Sci., v.39, pp.527-536.

Al-Heety, E. A. M. (2007) Historical seismicity of the stable Continental regions (SCRS) in the Arabian plate (preliminary study), Jour. Al-Anbar Univ. Pure Sci., v.1(1), pp.1-10.

Archuleta, R. J., Cranswick, E., Muellar, C. and Spudich, P. (1982) Source parameters of the 1980 Mammoth Lakes, California, Earthquake sequence, Jour. Geophys. Res., v.87, pp.4595–4607.

Assumpcao, M. (1998) Seismicity and stresses in the Brazilian passive margin, Bull. Seism. Soc. Amer., v.78(1), pp.160-169.

Assumpco, M., Schimmel, M. and Escalante. C. et. al. (2004) Intraplate seismicity in SE Brazil: stress concentration in lithospheric thin spots. Geophys. Jour. Internat., v.159, pp.390-399.

Behera, L., Sain, K. and Reddy, P.R. (2005) Evidence of underplating from seismic and gravity studies in the Mahanadi Delta of eastern India and its tectonic significance. Jour. Geophys. Res., v.109, pp.1-25.

Berteusen, K. A. (1977) Moho depth determinations based on spectral ratio analysis of NORSAR long-period P waves. Phys. Earth Planet. Interior, v.313, pp.13-326.

BruuBouchon, M. (1981) A simple method to calculate Green's functions for elastic layered media. Bull. Seismol. Soc. Amer., v.71, pp.959-971.

Brune, J. N. (1970) Tectonic stress and the spectra of seismic shear waves from earthquakes. Jour. Geophys. Res., v.75, pp.4997–5009.

Byerlee, J. (1978) Friction of rocks, Pure Appld.Geophys, v.116, pp.615-626.

Calais, E., Freed, A.M., Van Arsdale, R. and Stein, S. (2010) Triggereing of New Madrid seismicity by late –Pleistocene erosion, Nature, v.466, pp.608-611.

Campbell, D. L. (1978) Investigation of the stress –concentration mechanism for intraplate earthquakes, Geophys. Res. Lett., v.5, pp.477-479.

Chandra, U. (1977) Earthquakes of Peninsular India - a seismotectonic study, Bull. Seismol. Soc. Amer., v.67(5), pp.1387-1413.

Chetty, T.R.K. and Murthy, D.S.N. (1994) Regional tectonic framework of the Eastern Ghats Mobile Belt: a new interpretation. Proc. Workshop on Eastern Ghat Mobile Belt, Geol. Surv. India, v.44, pp.39-50.

Coutant, O. (1989) Program of numerical simulation AXITRA; Research Report, Laboratoire de Ge´ophysique Interne et Tectonophysique, Grenoble.

Dimri, V.P. (1992) Deconvolution and Inverse Theory: Application to Geophysical Problems, Elsevier Science Publishers, Amsterdam 230p.

Dunn, J.A. (1929) The geology of north Singhbhum. Mem. Geol. Surv. India, v.54, pp.166.

Fletcher, J. B. (1995) Source parameters and crustal Q for four earthquakes in South Carolina. Seismol. Res. Lett., v.66, pp.44-58.

Gangopadhyay, A. and Talwani, P. (2003) Symptomatic features of intraplate earthquakes, Seismol. Res. Lett., v.74, pp.863-883.

Ghosh, S.K. and Sengupta, S. (1990) The Singhbhum shear zone: structural transition and a kinematic model, Proc. Indian Acad. Sci., v.1, pp.229-247.

Gupta, S., Mohanty, W. K., Mandal, A. and Misra, S. (2014) Ancient terrane boundaries as probable seismic hazards: A case study from the northern boundary of the Eastern Ghats Belt, India. Geoscience Frontiers, v.5, pp.17-24.

Hanks, T. C. (1977) Earthquake stress drops, ambient tectonic stresses and stresses that drive plate motions, Pure Appld. Geophys., v.115, pp.441-458.

Havskov, J. and Ottemoller, L. (2003) SEISAN: the earthquake analysis software manual, pp.203.

Holdsworth, R.E., Hand, M., Miller, J.A. and Buick, I.S. (2001) Continental reactivation and reworking: an introduction. *In:* J.A. Miller, R.E., Holdsworth, I.S. Buick and M. Hand (Eds.), Continental Reactivation and Reworking. Geol. Soc. London, Spec. Publ., v.184, pp.1-12.

Johnston, A.C. and Kanter, L.R. (1990) Earthquakes in stable continental crust. Scientific American, v.262, pp.54-68.

Kanamori, H.K. and Anderson, D.L. (1975) Theoretical basis of some empirical relations in seismology, Bull. Seismol. Soc. Amer., v.65, pp.1073-1095.

Kayal, J. R., Srivastava, V. K., Bhattacharya, S. N., Khan, P. K. and Chatterjee, R. (2009) Source Parameters and Focal Mechanisms of Local Earthquakes: Single Broadband Observatory at ISM Dhanbad. Jour. Geol. Soc. India, v.74, pp.413-419.

Khan, P. K., Biswas, B., Samdarshi, P. and Prasad, R. (2011) Seismicity and the coda-Q variation in eastern Indian shield region, Indian Jour Geosci., v.65(2), pp.43-50.

Kikuchi, M. and Kanamori, H. (1991) Inversion of complex body waves, III, Bull. Seismol. Soc. Amer., v.81, pp.2335–2350.

Krishna, B.N. and Negi, J.G. (1973) Rift valleys beneath Deccan Trap, India. Geophys. Res. Bull. Hyderabad, v.11, pp.207-237.

Kumar, M., Yallanki, S., Biswas, K. and Mandal, P. (2015) Evidence for non-self-similarity in the Mw7.7 2001 Bhuj earthquake sequence, Natural Hazards, v.75, pp.1577-1598 (DOI 10.1007/s11069-014-1381-3).

Lenardic, A., Moresi, L. and Muhlhaus, H. (2000) The role of mobile belts for the longevity of deep cratonic lithosphere: the crumple zone model, Geophys. Res. Lett., v.27, pp.1235-1238.

Mahapatro, S. N., Tripathy, A. K., Nandi, J. K. and Roy, A. (2009) Coexisting Ultramylonite and Pseudotachylyte from the Eastern Segment of the Mahanadi Shear Zone, Eastern Ghats Mobile Belt. Jour. Geol. Soc. India, v.74, pp.679-689.

Malservisi, R., Hugentobler, U., Wonnacott, R. and Hackl, M. (2013) How rigid is a rigid plate? Geodetic constraint from the TrigNet CGPS network, South Africa, Geophys. Jour. Internat., v.192(3), pp.918-928.

Mandal, P., Manglik, A. and Singh, R. N. (1997) Intraplate stress distribution beneath the Killari region, India. Jour. Geophy. Res., v.102(11), pp.719-729.

Mandal, P., Srivastava, J., Joshi, S., Kumar, S., Bhunia, R. and Rastogi, B.K. (2004) Low coda-Qc in the epicentral region of the 2001 Bhuj Earthquake of Mw 7.7, Pure Appld. Geophys., v.161, pp.1635-1654.

Mandal, P. and Biswas, K. (2016) Teleseismic receiver function modeling of the eastern Indian craton, Phys. Earth Planet. Int., DOI: 10.1016/j.pepi.2016.07.002.

Mandal, P., Singh, B., Gupta, A., and Nagendra, P. (2017) Modeling of source parameters of the 15 December 2015 Deogarh earthquake of M_w4.0, Jour. Geol. Soc. India, v.89, pp.363-368. DOI:10.1007/s12594-017-0616-9

Mazumder, R., Van Loon, A. J., Mallik, L., Reddy, S. M., Arima, M., Altermann, W., Eriksson, P. G. and De, S. (2012) Mesoarchaean-Palaeoproterozoic stratigraphic record of the Singhbhum crustal province, eastern India: a synthesis; *In:* Mazumder, R. and Saha, D. (Eds.) Palaeoproterozoic of India. Geol. Soc. London, v.365, pp.31-49.

Mohanty, W. K., Prakash, R., Suresh, G., Shukla, A. K., Yanger Walling, M. and Srivastava, J. P. (2009) Estimation of Coda Wave Attenuation for the National Capital Region, Delhi, India Using Local Earthquakes, Pure Appld. Geophys., v.166, pp.429-449.

Mooney, W. D., Ritsema, J. and Hwang, Y. (2012) Crustal seismicity and maximum earthquake magnitudes (Mmax) in stable continental regions (SCRs): correlation with the seismic velocity of the lithosphere. Earth Planet. Sci. Lett., v.357/358, pp.78-83.

Morgan, W. J. (1968) Rises, trenches, great faults, and crustal blocks. Jour. Geophys. Res., v.73, pp.1959-1982.

Morrow, C., Radney, B. and Byerlee, J.D. (1992) Frictional strength and the effective pressure law of montmorillonite and illite clays: fault mechanics and transport properties of rocks. *In:* Evans, B. and Wong, T.F. (Eds.), Fault Mechanics and Transport Properties of Rocks. Academic Press, San Diego, California, pp.69-88.

Mukhopadhyay, J., Beukes, N.J., Armstrong, R.A., Zimmermann, U., Ghosh, G. and Medda, R.A. (2008) Dating the oldest Greenstone in India: a 3.51 Ga precise U-Pb SHRIMP Zircon Age for Dacitic Lava of the Southern Iron Ore Group, Singhbhum Craton, Jour. Geol., v.116, pp.449-461.

Naqvi, S.M. and Rogers, J.J.W. (1987) Precambrian Geology of India. Oxford Univ. Press Inc. 223p.

Oldham, T. (1883) A catalogue of Indian earthquakes from the earliest times to the end of 1869 A.D., Mem. Geol. Surv. India., v.XIX, Part 3.

Rajendran, C.P., Rajendran, K. and John, B. (1996) The 1993 Killari (Latur) central India earthquake: an example of fault reactivation in Precambrian crust, Geology, v.24(7), pp.651-654.

Rajendran, C. P., Rajendran, K., Thakkar. M. and Goyal, B. (2008) Assessing the previous activity at the source zone of the 2001 Bhujearthquake based on the near-source and distant paleo-seismological indicators. Jour. Geophys. Res., v.113, pp.1-17.

Saha, A.K. (1994) Crustal evolution of Singhbhum–North Orissa, Eastern India. Mem. Geol. Soc. India, no.27, pp.341.

Saha, A., Lijesh, S. and Mandal, P. (2012) Simultaneous estimation of earthquake source parameters and crustal Q value from broadband data of selected aftershocks of the 2001 Mw 7.7 Bhuj earthquake, Jour. Earth Syst. Sci., v.121, pp.1421-1440.

Sandiford, M .and Egholm, D. L. (2008) Enhanced intraplate seismicity along continental margins: Some causes and consequences. Tectonophysics, v.457, pp.197-208.

Sarkar, A.N. (1982) Precambrian tectonic evolution of eastern India: A model of converging microplates. Tectonophysics, v.86, pp.363-397.

Sarkar, A.N. and Chakraborty, D.K. (1982) One orogenic belt or two? A structural reinterpretation supported by Landsat data products of the Precambrian metamorphics of Singhbhum, Eastern India, Photogrammetria, v.37, pp. 185-201.

Savage, J.C. and Wood, M.W. (1971) The relation between apparent stress and stress drop. Bull. Seism. Soc. Amer., v.61, pp.1381-1386.

Schulte, S.M. and Mooney, W.D. (2005) An updated global earthquake catalogue for stable continental regions: reassessing the correlation with ancient rifts, Geophys. Jour. Internat., v.161, pp.707-721.

Seismic Analysis Code (SAC2000) 2000(http://www.iris.edu/manuals/sac/SAC_Home_Main.html)280.

Sibson, R. H. (1984) Roughness at the base of the seismogenic zone: contributing factors. Jour. Geophys. Res., v.89, pp.5791-5799.

Singh, S.K. and Ordaz, M. (1994) Seismic energy release in Mexican subduction zone earthquakes, Bull. Seismol. Soc. Amer., v.84(5), pp.1533-1550.

Singh, S.K., Bansal, B.K., Bhattacharya, S.N., Pacheco, J.F., Dattatrayam, R. S., Ordaz, M., Suresh, G., Kamal, and Hough, S.E. (2003) Estimation of Ground Motion for Bhuj (26 January 2001; Mw 7.6) and for Future Earthquakes in India, Bull. Seismol. Soc. Amer., v.93(1), pp. 353–370.

Singh, S.K., Garcia, D., Pacheco, J.F., Valenzuela, R., Bansal, B.K. and Dattatrayam, R.S. (2004) Q of the Indian Shield, Bull. Seismol. Soc. Amer., v.94(4), pp.1564–1570.

Sokos, E. N. and Zahradník, J. (2008) ISOLA a FORTRAN code and a MATLAB GUI to perform multiple-point source inversion of seismic data. Comput. Geosci., v.34, pp.967–977.

Sokos, E. N. and Zahradník, J. (2013) Evaluating Centroid-Moment-Tensor uncertainty in the new version of ISOLA software, Seismol. Res. Lett., v.84(4), pp. 656-665.

Sykes, L. (1978) Intraplate seismicity, reactivation of pre-existing zones of weakness, alkaline magnetism, and other tectonism postdating continental

fragmentation. Reviews of Geophysics and Space Physics, v.16, pp.621-688.

Tait, J., Zimmermann, U., Miyazaki, T., Presnyakov, S., Chang, Q., Mukhopadhyay, J. and Sergeev, S. (2011) Possible juvenile Palaeoarchaean TTG magmatism in eastern India and its constraints for the evolution of the Singhbhum craton, Geological Magazine, v.148, pp.340-347.

Talwani, P. (1999) Fault geometry and earthquakes in continental interiors. Tectonophysics, v.305, pp.371-379.

Zahradnik, J., Serpetsidaki, A., Sokos, E. and Tselentis, G.A. (2005) Iterative deconvolution of regional waveforms and a double-event interpretation of the 2003 Lefkada Earthquake, Greece, Bull. Seismol. Soc. Amer., v.95(1), pp.159–172.

Zuniga, F. R. (1993) Frictional overshoot and partial stress drop, which one? Bull. Seismol. Soc. Amer., v.83, pp.939-944.

(Received: 28 March 2016; Revised form accepted: 1 August 2016)